Modelling different penetration rates of automated eco-driving electric vehicles in an urban area

Jakub Krol, Bani Anvari, Craig Rafter, James Fleming, Xingda Yan and Roberto Lot

***Abstract*—Eco-driving strategies have proven to be effective in providing energy savings for the vehicle that is utilising them. This paper explores the underinvestigated impact of eco-driving vehicles on other network participants adhering to conventional driving styles. An eco-driving strategy designed for an electric vehicle that trades off energy savings with naturalistic driving without relying on vehicle-to-infrastructure or vehicle-to-vehicle communication is extended using Gaussian Process Regression for real-time predictive speed optimization. It enables the assessment of its network effects in two scenarios: 1) a platoon and 2) an urban network simulation with mixed-mode traffic and varying demand levels. Initial validation involves an eco-driving vehicle responding to a platoon leader, influencing following vehicles governed by the Intelligent Driver Model (IDM). Further analysis introduces eco-vehicles into an IDM-governed network under different traffic conditions. Energy savings of up to 21% were achieved in cars following a vehicle that prioritises energy savings and, of up to 13% if they followed a vehicle that attempts to balance energy savings and conventional driving style. In the urban scenario, positive effects on other users are observed in high density traffic even if only a small number of eco-vehicles are present in the network. The largest energy savings achieved in conventional vehicles were 5.1% and were obtained for high-density traffic and a network consisting of 25% of eco-vehicles.**

***Index Terms*—Eco-driving, Electric vehicles, ADAS, Energy efficiency, Driver satisfaction, Speed optimisation**

I. Introduction

Road vehicles emit atmospheric pollutants such as Carbon dioxide (CO_2) carbon monoxide (CO), Nitrogen oxides (NO_x) and particulate carbon. In 2019, it was reported that the transport sector is responsible for about 30%, 33%, 24% of the Europes, UK's and global CO_2 emissions respectively, of which the majority comes from road transportation [1]. Changing the energy source of the majority of the road vehicles via introduction of electric vehicles (EVs) is considered to be a feasible and sustainable way to reduce harmful emissions [2].

Nonetheless, the need to make EVs more energy efficient persists, since current vehicles are characterised by short battery life and consequently a shorter driving range [3]. Also, slow charging cycles and lack of charging infrastructures is often raised as an issue by potential users and hinders the adoption of EVs [4]. Furthermore, reduction of an amount of charge cycles improves battery health [5] and will reduce load on the electricity network [6].

Research has estimated that 5-10% of fuel can be saved if drivers pursue a more energy efficient, economical and environmentally friendly driving style referred to as eco-driving [7], [8], [9], which is characterised by behaviours such as modest acceleration, early gear changes, minimisation of unnecessary braking/stopping, and driving below the speed limit. Compared to hardware-based energy reduction approaches, eco-driving can be immediately applied to any vehicle [10]. Eco-driving not only has benefits in reducing fuel consumption and noxious emissions of conventional vehicles, but also has applications for EVs, where a reduction in electrical energy usage leads to an increase in the driving range and reduction in frequency of charge cycles [11].

Despite the evidence demonstrating that controlled vehicles can achieve a reduction in energy consumption, the impact of eco-driving cars on network behaviour has not been extensively studied. Previous studies have investigated the formulation of optimisation problems involving conventional vehicles following eco-driving cars [12], [13], leading to an increase in complexity. Furthermore, these studies assume the existence of vehicle-to-infrastructure (V2I) and vehicle-to-vehicle (V2V) communication, which is not yet widely adopted.

This study focuses solely on the optimisation of an eco-driving vehicle and examines how other vehicles in a network adjust their response and if it leads to savings in their energy consumption. It is not clear if the eco-driving behaviour would be followed by other vehicles or if it would possibly lead to energy consumption increases, travel delays or traffic instabilities. For example, slow acceleration, even though beneficial for an individual vehicle in terms of energy usage, can lead to congestion, increasing overall consumption.

Furthermore, it is expected that the impact of eco-driving on other vehicles will heavily depend on the underlying traffic conditions. It is not necessarily clear whether eco-driving in congested conditions will alleviate the resulting energy wastage or aggravate the issue. For example, in congested scenarios drivers will be constrained by the behaviour of the vehicle in front of them, which can possibly lead to imitation of the ecological driving strategy.

In this paper, the impact of eco-driving behaviour on other

Manuscript received ...; revise d .... ; accepted .... This research is funded by the EPSRC [grant No.: EP/N022262/1] and T-TRIG 2019 by DfT whose supports are gratefully acknowledged. The dataset and code used in this study is publicly available at: https://rdr.ucl.ac.uk/.

Jakub Krol and Bani Anvari are with Centre for Transport Studies, Faculty of Eng., UCL, UK j.krol@ucl.ac.uk; b.anvari@ucl.ac.uk

Craig Rafter is with Faculty of Eng. & the Environment, University of Southampton, UK

James Fleming is with Electrical and Manufacturing Eng., Loughborough University, UK

Xingda Yan is with Connected Places Catapult, UK

Roberto Lot is with Department of Industrial Eng., University of Padova, Italy

car drivers in the network is investigated using a unique eco-driving model on a large scale realistic case study. A model of eco-driving is adopted which trades-off the minimisation of energy usage with a naturalistic driving style. The effects of this model are investigated in two scenarios, in vehicle platoons and in an urban network.

The contributions of this paper are as follows:

- An eco-driving model, that includes trade-off of energy usage with a naturalistic style, is adopted and extended by introducing a Gaussian Process Regression for real-time predictive speed optimisation.
- The framework for analysing any eco-driving strategy and its network impact is developed based on realistic urban scenario.
- The impact of proposed eco-driving behaviour on other vehicles in the network is investigated on two case studies: 1) a vehicle platoon and 2) an urban network (a large-scale realistic simulation case study which accounts for mixed-mode traffic and multiple levels of traffic demand).

The structure of the paper is as follows: Section II provides an overview of state-of-the-art eco-driving strategies and highlights the gap. The approach used in this paper is based on optimal control theory and is explained in Section III. The methodology used to investigate the impact of eco-drivers on other vehicles is outlined in Section IV. The proposed model is tested on two case studies, and the results are discussed in Sections V and VI. Conclusions and future avenues of research are summarised in Section VII.

II. Literature Review

a) Eco-driving strategies: Finding the most energy-efficient behaviour in a given driving scenario may be considered as an optimal control problem [14]. For example, it can be used to calculate optimal trajectories for driving scenarios such as acceleration to cruise speed, driving between stop points or cruising on hilly terrain while maintaining a given average speed [15]. However, effective eco-driving needs to adapt to road conditions and the behaviour of the vehicle ahead, where predetermined strategies may not be sufficient. A centralised optimal control problem can be solved to recommend speed profiles for network participants using traffic and geographical information [16]. Nonetheless, the coordination between all network participants is not currently viable. In order to address those difficulties, separate optimal control problems can be solved for each vehicle in an online setting, responding to instantaneous circumstances. An example is the calculation of energy optimal torque split, gear shift, and velocity control input of a parallel Hybrid Electric Vehicle (HEV) using Model Predictive Control (MPC) [17].

Since most eco-driving approaches try to avoid braking as much as possible, some anticipation of the motion of preceding vehicles is required by either the driver or the assistance system. In dynamic eco-driving systems, advice based on real-time traffic information is given to the driver, contributing to reductions of energy consumption of 10% to 20% in highway driving situations [18]. Information about the velocity of a leading vehicle can be conveyed through vehicle-to-vehicle communication and subsequently used to impose safety constraints. For eco-driving assistance systems that solve the problem in real-time based on sensor data, safety constraints can be incorporated into the optimal control problem, for example by constraining the space gap distance to be greater than a safe value. For most problems, numerical solution methods are required; nonetheless, analytical solutions exist in some simple cases [14], [19]. An extensive review of eco-driving strategies, including cooperative driving and incorporation of environment information, is given in [20].

b) Driving comfort: Naturalistic driving typically differs from eco-driving as the driver may not be aware of eco-driving techniques, and even then techniques are sometimes difficult to apply in practice due to the need to anticipate traffic flow [7], which makes optimal coasting behaviour difficult to achieve without assistance. Furthermore, optimal eco-driving solutions typically do not respect driver preferences on following distance, longitudinal and lateral accelerations and cornering speeds. It is possible to account for these preferences explicitly in the optimal control problem for energy minimisation by augmentation of the cost function, leading to optimal control formulations that can trade off fuel savings with driver preferences [21].

c) Energy Management of electric vehicles: Recent advancements in energy management strategies for Connected and Autonomous Electric Vehicles have led to significant improvements in energy efficiency. These advancements utilise innovative optimisation algorithms and data integration techniques, enhancing performance across various driving environments. A systematic review in [22] explores control methods and optimisation for extended-range electric vehicles, aiming to maximise fuel economy and enhance performance. A key development is the energy-aware optimisation (EAO) strategy, which focuses on the vehicle-traffic nexus, as shown in [23]. This strategy uses a bias deep compensative estimator for vehicle dynamics model parameter identification, achieving over a 7.5% relative energy-saving compared to traditional methods, highlighting the benefits of integrating vehicle-traffic interactions into energy optimisation. Furthermore, an in-vehicle energy optimal control system developed in [24] operates the motor drive system at high efficiency, extending the driving range and outperforming model predictive control methods. Additionally, a multi-lane hierarchical optimisation (MLHO) algorithm in [25] utilises vehicle-to-everything communication for hybrid electric vehicles (HEVs), integrating speed planning and energy management to improve fuel economy by 32% over human-driven models. A predictive energy management strategy (EMS) for connected plug-in hybrid electric vehicles (PHEVs) in [26] employs a wavelet neural network optimised by a particle swarm optimisation algorithm, significantly enhancing fuel economy by utilising dynamic traffic information. On the safety and optimisation front, a two-stage decision-making framework in [27] balances safety with energy efficiency in vehicle-following scenarios. An energy-saving optimisation and control (ESOC) method for Autonomous Electric Vehicles in [28] integrates driving scene constraints into vehicle dynamics, optimising powertrain efficiency and surpassing existing methods. Lastly, an energy

conservation control (ECC) system in [29] optimises energy consumption on sloped roads by estimating a vehicle's total mass and pitch angle in real-time, showing improved performance over traditional cruise control.

d) Network impact: Besides the benefit of eco-driving for individual vehicles, eco-driving can impact the emissions and traffic flow of other vehicles at low to medium levels of traffic demand. In [30], [31], [32], eco-driving is incorporated by providing upper bounds on maximum acceleration without any additional penalty on space headway and the impact of eco-vehicles on conventional vehicles is analysed in a small number of studies. At times of high demand, high penetrations of eco-drivers can result in negative effects by increasing congestion and reducing capacity [30]. More specifically, Garcia-Castro et al. [30] showed that under low and medium congested traffic conditions, eco-driving leads to reductions of up to 2.3% in CO_2 and of up to 4.3% in NO_x emissions per km. Nonetheless, under highly-congested traffic conditions, emissions increase by up to 1.3% and 0.5%, respectively. Findings in [30] replicate those in [31], [32] where increase in emissions was observed for heavy-traffic volumes. In [33], the problem of approaching a signalised intersection was considered and a penalty on large space headway to the preceding vehicle was enforced. In this study, energy reductions were retained for a high percentage of eco-driving vehicles even during over-saturated conditions. It was observed that the improvements level off at around 40% penetration rate of eco-driving vehicles.

A similar study was performed in [34] for Hybrid Electric Vehicles (HEVs) and a 3% decrease in total energy consumption and emissions was achieved using an eco-driving strategy supplemented by information from vehicle-infrastructure communication, such as traffic light stages. Furthermore, it was demonstrated in [34] that the benefit-cost ratio exceeds one for penetration rates larger than 20% plug-in HEVs or 30% HEVs. The optimal control problem used in [35] incorporates only the fuel minimisation without taking into account driver comfort. Eco-driving can also reduce traffic shock wave propagation as drivers adjust their behaviour to smoother acceleration and less braking [36].

III. Eco-driving model for a single vehicle

The eco-driving strategy explained in Sections III-A to III-C is based on optimal control theory and was first introduced in [37]. The idea is to minimise a penalty function that blends two conflicting objectives: satisfying driver preferences, which is illustrated in Section III-A, and reducing vehicle energy usage, which is described in Section III-B. At each time instance, t_n, the optimisation problem defined in Section III-C is solved, which outputs the vehicle control input that the driver should apply over a future time horizon, t_h. Three driving styles are considered here for calculating the total energy consumption. Section III-D explains a new technique for real-time predictive speed optimisation. The proposed method allows assessing the impact of eco-drivers on traffic and energy consumption in an urban network.

TABLE I: Notations

Variable	Explanation
x_i	Location of vehicle i
v_i	Velocity of vehicle i
a_i	Longitudinal acceleration of vehicle i
x_{i-1}	Location of the lead vehicle $i-1$
v_{i-1}	Velocity of the lead vehicle $i-1$
a_{i-1}	Longitudinal acceleration of the lead vehicle $i-1$
v_d	Desired free-flow velocity
v_{max}	Speed limit on a road segment
Δv	Relative velocity
a_{max}	Maximum acceleration
b	Comfortable breaking deceleration
l_l	Length of a lane
l_k	Lengthscale hyperparameter of Radial Basis Function (RBF) kernel
L_d	Driver i's penalty function
δ	Exponent
s	Space gap between two consecutive vehicles
s_d	Speed-dependant desired safe space gap between two vehicles
s_0	Minimum space gap
s_{max}	Maximum space gap
$s_{junction}$	Space gap between a vehicle and a junction
S_{DSM}	Set of parameters in Driver Satisfaction Model (DSM)
S_{IDM}	Set of parameters in Intelligent Driver Model (IDM)
m	Mass
F	Driving force
$c_d v^2$	Aerodynamic drag
c_{rr}	Rolling resistance
T	Motor torque
T_{min}	Minimum motor torque
T_{max}	Maximum motor torque
t_0	Safe time headway
t_h	Future time horizon
t_n	Current time
t_f	Final time of a journey
Δt	Time interval of 0.1
B	Braking torque
η_t	Efficiency of the transmission
η_e	Efficiency of the electric battery
N	Gear ratio of the transmission
r	Rolling radius of the tyres
β	Braking force
ω	Motor angular velocity
i_b	Battery current
E_0	Open circuit voltage
P_b	Power
L	Eco-driving objective function
α	Trade-off parameter
E	Energy usage per-distance travelled
E_n	Network energy consumption
E_{ref}	Total energy consumption of the real vehicle
$E_{n,ref}$	Network energy consumption for scenario without eco-vehicles
ΔE	Relative energy improvement
ξ	Data point for Gaussian Process Regression (GPR)
p	Number of inputs to the GPR
M	Number of data points used to train the GRP model
$M*$	Number of data points during the application of the GPR model
τ	The uncertainty threshold in the GPR model
σ_n	Variance of additive i.i.d. Gaussian noise
l_k	Lengthscale hyperparameter
k	Kernel function in GPR
K	Covariance matrix in GPR
$\boldsymbol{X}$	Reference input used to train GPR
$\boldsymbol{y}$	Reference output used to train GPR
$\hat{\boldsymbol{f}}$	Prediction generating function in GPR
$\hat{\sigma}$	Uncertainty generating function in GPR
σ	Uncertainty of GPR prediction
$v^*_{t_n}$	Solution to OCP problem at time t_n
$\hat{v}_{t_n}$	GPR prediction at time t_n
κ	A random variable
ρ	Pearson's correlation coefficient of variables travel time & energy consumption over a common travelled distance
t_x	Travel time over a common travelled distance

A. Driver Satisfaction Model (DSM) with eco-driving

The dynamics of a road vehicle i moving along a prescribed trajectory can be described by differential equations:

$$\dot{x}_i = v_i \tag{1}$$

$$\dot{v}_i = a_i \tag{2}$$

where x is the position along a trajectory, v the velocity and a the longitudinal acceleration, which is chosen by the driver.

When driving in traffic, it is essential to maintain a safe space gap s from any leading vehicle $i-1$, which may be calculated by integration as in:

$$\dot{s}_i = v_{i-1} - v_i \tag{3}$$

Here, v_{i-1} is the velocity of the leading vehicle. From a control perspective, changes to this velocity, i.e. leader acceleration, can be considered as an unmodelled disturbance.

In the literature, there are several driver models that aim to mimic human driving behaviour, one of the most popular in traffic simulation is the Intelligent Driver Model (IDM) [38]. In [39] we developed an alternative model based on optimal control theory, which extends the car-following capabilities of the IDM to consider cornering and fuel economy targets. Regarding car-following behaviour, we developed a penalty function that, minimised over a time interval, induces a realistic driver behaviour and which gives similar mean squared errors to the IDM when validated using real-world data [39]. Following [39], the *driver preference* penalty depends on the vehicle state s_i, v_i and acceleration input a_i as follows:

$$\begin{aligned} L_d = &\left(a_i/a_{\max}\right)^2 + \delta^2 (v_i/v_d - 1)^2 \\ &+ 8\left((v_{i-1}/v_d)^{\delta} - 1\right)^2 \frac{(s/s_d - 1)^2}{(s/s_d)^2 + 1} \end{aligned} \tag{4}$$

where the first term applies a penalty to acceleration (the control action) with larger values of $a_{\max}$ giving lower penalties, while the second term introduces a penalty when the actual speed is different from the desired free-flow velocity v_d. The final term is a soft constraint that is used to keep the space gap greater than a speed-dependent safe space gap $s_d = v_i t_0 + s_0$ (where t_0 and s_0 are constant), which may be occasionally overruled if emergency braking is necessary to avoid collisions, which is enforced by the constraint:

$$s \geq 0 \tag{5}$$

During the optimisation, the acceleration a_i in (4) is upper bounded such that:

$$a_i \leq a_{\max}, \tag{6}$$

while no lower limit is considered to allow possible emergency braking. Additionally, an upper bound on velocity is introduced in order to comply with speed limits:

$$v_i \leq v_{\max}, \tag{7}$$

In summary, driver preferences are summarised with a set of four constant parameters:

$$S_{\text{DSM}} = (v_d, a_{\max}, t_0, s_0), \tag{8}$$

which may be adjusted to match a particular driver if desired, and are a subset of the parameters used in the IDM [38].

B. Energy usage of the electric vehicle

The vehicle is modelled as a mass subject to Newton's laws of motion,

$$m\dot{v} = F - \text{sign}(v)(c_d v^2 - c_{rr}), \tag{9}$$

where v is the vehicle speed, F is the driving force, $c_d v^2$ is the aerodynamic drag, and c_{rr} is the rolling resistance. Although the vehicle acceleration $\dot{v}$ is physically determined by the driving force F, we use the acceleration $a = \dot{v}$ as the control input. In this way, we can immediately link the vehicle model to the driver model in Section III-A. Therefore, the driving force becomes an output of the controlled system:

$$F = ma + c_d v^2 + c_{rr}, \tag{10}$$

where, for simplicity, we have assumed $v > 0$.

Figure 1 shows the architecture of a modern electric vehicle, which typically consists of an electric battery and a single electric motor, which is connected to the driving axle by a single reduction gear. The overall driving force is the sum of the motor torque T and the braking torque B

$$F = \frac{B + \eta_t N T}{r} \tag{11}$$

here η_t and N are the efficiency and gear ratio of the transmission respectively, while r is the rolling radius of the tyres. In EVs, it is possible to recover energy by combining the action of brakes and electric motor. Energy recovery is subject to several limitations (such as tyre friction on each axle, motor torque and power, battery power). For simplicity, we assume that a fixed proportion $0 \leq \beta \leq 1$ of the braking force is applied by the motor. In summary, in order to achieve the acceleration a at the current speed v, the motor must provide a torque:

$$T(v, a) = \frac{r}{N}\left[\frac{\max(F, 0)}{\eta_t} + \eta_t \beta \min(F, 0)\right] \tag{12}$$

where the transmission efficiency is assumed to be the same as in the forward direction. Moreover, the motor angular velocity reads

$$\omega(v) = \frac{Nv}{r}. \tag{13}$$

The efficiency of the energy conversion from electrical to mechanical, in other words the combined efficiency of the battery, power converter, and motor, is

$$\eta(\omega, T) = \frac{T\omega}{i_b E_0} \tag{14}$$

where i_b and E_0 are the battery current and open circuit voltage respectively. Hence, we can calculate the battery power usage from Equation (14) and power P_b is expressed as a function of vehicle speed and acceleration:

$$P_b(v, a) = \frac{T(a, v)\omega(v)}{\eta(a, v)} \tag{15}$$

In order to solve the optimal control problem, we have predetermined the power map, $P_b(v, a)$, by estimating the current usage of the electric motor and inverter of a 2019 Nissan Leaf. The power map is depicted in Figure 2. For optimal control,

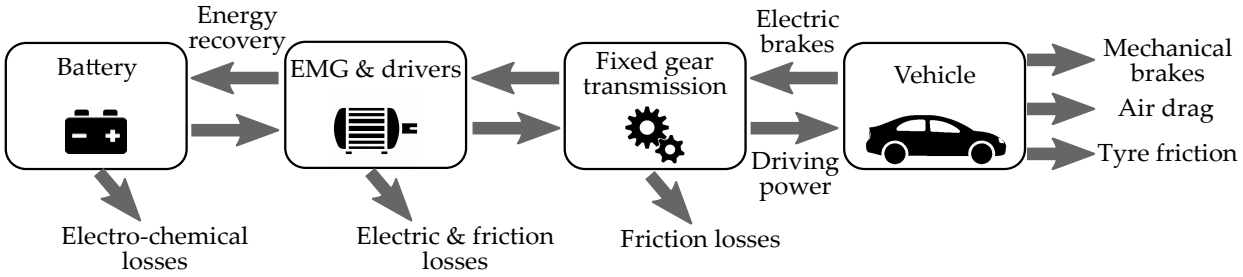

Fig. 1: The architecture of an electric vehicle's powertrain.

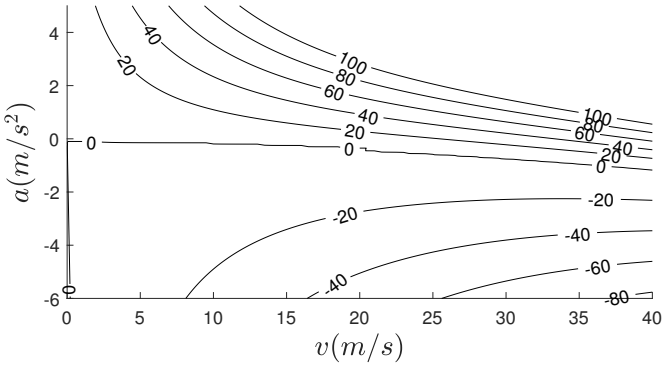

Fig. 2: Battery power, P_b, as a function of the vehicle speed and acceleration (the battery is discharging when $P_b > 0$ and recharging when $P_b < 0$).

the power map is approximated by the following quadratic polynomial:

$$P_b(v, a) = p_a a + q_{av} av + q_{vv} v^2. \tag{16}$$

During the optimisation, we also take into account limits on torque and power of the electric motor:

$$T_{\min} \leq T \leq T_{\max} \tag{17}$$

$$|T\omega| \leq P_{\max} \tag{18}$$

C. Balancing energy efficiency and driver preference via optimal control

We now combine the driver preference and vehicle power usage into a single function by introducing a trade-off parameter α

$$L(s, v, a) = L_d(s, v, a) + \alpha \frac{P_b(v, a)}{P_{\max}} \tag{19}$$

where power P_b has been divided by its maximum in order to make the function L dimensionless. In summary, the optimal control problem reads

$$\begin{aligned} \min_{a(t)} \quad & \int_0^{t_f} L(s, v, a)\, \mathrm{d}t \\ & + \frac{\alpha}{10^6}(x(t_f) - v_d t_f)^2 \\ \text{subject to} \quad & \dot{x} = v, \dot{v} = a, \dot{s} = v_{i-1} - v_i \\ & x(0) = 0, v(0) = v_0, s(0) = s_0 \\ & (5),\ (6),\ (7),\ (17),\ (18) \end{aligned} \tag{20}$$

where a terminal cost, $(x(t_f) - v_d t_f)^2$, is introduced to penalise solutions that travel excessively slowly. By setting $\alpha = 0$, the solution to (20) becomes very similar to the IDM car-following model. As α increases, the energy usage becomes progressively more important and the solution of the Optimal Control Problem (OCP) moves towards an eco-driving behaviour. The absolute minimum of energy usage can be found when $\alpha \to \infty$, but in any case the term L_d must be included in the penalty (19) in order to avoid the potential collision with the preceding vehicle.

The optimisation problem (20) often cannot be solved in real-life, since it requires a knowledge about the future speed profile of the lead vehicle v_{i-1} over a whole trip duration t_f. Therefore, the solution to the optimal control problem must be solved over a significantly shorter future time horizon, t_h, and repeatedly recalculated in a receding horizon manner. A terminal cost is modified accordingly and the receding horizon problem is formulated, as

$$\begin{aligned} \min_{a(t)} \quad & \int_{t_n}^{t_n + t_h} L(s, v, a)\, \mathrm{d}t \\ & + \frac{\alpha}{10^6}(x(t_n + t_h) - x(t_n) - v_d t_h)^2. \end{aligned} \tag{21}$$

It should be noted that in cases where $\alpha = 0$ and terminal cost has no effect, the vehicle is still travelling forward as any diversions from v_d and large values of s_d are penalised in the L_D term of the objective function.

This formulation allows for simple assumptions on lead vehicle dynamics, for example by setting v_{i-1} to be constant. In this case, solution to problem (21) should be computed at a sufficiently high rate in order to react to the changes in the leader velocity and prevent collisions. In an urban network scenario (see Section VI-A), the velocity update is done every 0.1 s, for a temporal resolution of 0.1 s and $t_h = 60$ s.

Three driving styles are considered for solving the OCP, which are explained below:

1) NATURAL ($\alpha = 0$): NATuralistic driving style, maximises the driving comfort without paying specific attention to energy economy;
2) ECO ($\alpha = 3.14 \times 10^8$): ECO-driving style characterised by energy minimisation, with the no-collision constraint (5) for ensuring safety;
3) BALANCED ($\alpha = 1.26 \times 10^6$): a trade-off case between the two aspects.

For each simulation, the driving efficiency is assessed in terms of the energy usage per distance travelled, which is

calculated as:

$$E = \frac{\int_0^{t_f} P_b(v,a)\,\mathrm{d}t}{x(t_f)} \tag{22}$$

The relative energy consumption ΔE is also defined as:

$$\Delta E = \frac{E_{ref} - E}{E_{ref}}, \tag{23}$$

where E_{ref} is the total energy usage of the simulations without eco-vehicles.

D. Approximation for obtaining real-time solutions

The computational cost of solving (21) increases rapidly when a large number of vehicles are considered simultaneously. On a standard laptop, computing the solution to (21) takes approximately 5.5 seconds. Running an urban network simulation with a time step of 0.1 seconds necessitates solving this problem ten times per simulation second for each vehicle, which takes about 55 seconds. For instance, if 20 vehicles are following the eco-driving strategy, the total computational time required to solve (21) for all of them will be approximately 1100 seconds or 18.3 minutes. This cost is prohibitively expensive, making it impractical to run simulations for a sufficient duration to obtain statistically meaningful comparisons.

Hence, for an urban network scenario, the computation time can be reduced by approximating (21) with an interpolation of previously obtained solutions. In order to apply such a technique, the number of independent variables in the model is reduced by assuming that $\partial v_{i-1}/\partial t = 0$, and appropriate subset of vehicles is associated with the same energy consumption map. In such a case, input is composed of four scalar values: $s(t_n)$, $v_{i-1}(t_n)$, $v_i(t_n)$, v_{max}.

In selecting an appropriate interpolation methodology, two conditions have to be satisfied:

1) The interpolation should happen on an unstructured data. A choice of appropriate rectangular grid for a case study is not trivial as the input space will not be uniformly distributed and in certain regions of the input space, a greater accuracy is required (e.g. when s is small);
2) The uncertainty of the interpolation should be low. In case of high uncertainty, (21) should be solved instead. Hence, the uncertainty of the interpolation should be calculated continuously.

Based on these considerations, Gaussian Process Regression (GPR) [40] is used. The GPR is a non-parametric, Bayesian approach to regression problems. It has the following advantages: 1) its prediction is obtained based on the interpolation of the past observations, 2) the prediction is probabilistic and Gaussian which allows calculation of the empirical confidence interval, and 3) it allows for nonlinear predictions by introducing a kernel function, $k(\boldsymbol{\xi}_i, \boldsymbol{\xi}_j)$, which specifies a similarity of two data points, $\boldsymbol{\xi}_i$ and $\boldsymbol{\xi}_j$.

A set of past observations consists of inputs $\boldsymbol{X} = [\boldsymbol{\xi}_1, \cdots, \boldsymbol{\xi}_M] \in \mathbb{R}^{p\times M}$ with associated outputs $\boldsymbol{y} \in \mathbb{R}^M$, characterised by mean value $\mu = \mathbb{E}(\boldsymbol{y})$ and input covariance matrix, $\boldsymbol{K}(\boldsymbol{X},\boldsymbol{X}) \in \mathbb{R}^{p\times M}$, where $K_{ij} := k(\boldsymbol{\xi}_i, \boldsymbol{\xi}_j)$. For a new set of samples, $\boldsymbol{X}^* \in \mathbb{R}^{p\times M^*}$, the approximation $\hat{\boldsymbol{f}}(\boldsymbol{X}^*) \in \mathbb{R}^{M^*}$ and the corresponding confidence intervals $\hat{\boldsymbol{\sigma}}(\boldsymbol{X}^*)$, are given by

$$\begin{aligned}\hat{\boldsymbol{f}}(\boldsymbol{X}^*) &= \boldsymbol{K}(\boldsymbol{X}^*,\boldsymbol{X})\boldsymbol{K}_\sigma^{-1}(\boldsymbol{X},\boldsymbol{X})(\boldsymbol{y}-\mu),\\ \hat{\boldsymbol{\sigma}}(\boldsymbol{X}^*) &= \mathrm{diag}(\boldsymbol{K}(\boldsymbol{X}^*,\boldsymbol{X}^*) - \\ &\qquad \boldsymbol{K}(\boldsymbol{X}^*,\boldsymbol{X})\boldsymbol{K}_\sigma^{-1}(\boldsymbol{X},\boldsymbol{X})\boldsymbol{K}(\boldsymbol{X},\boldsymbol{X}^*)),\end{aligned} \tag{24}$$

where $\boldsymbol{K}_\sigma(\boldsymbol{X},\boldsymbol{X}) = \boldsymbol{K}(\boldsymbol{X},\boldsymbol{X}) + \sigma_n^2\boldsymbol{I}$ and σ_n is variance of additive i.i.d. Gaussian noise in the model. In the following analysis, it is assumed that solutions to (21) are noise free, but $\sigma_n = 10^{-4}$ in order to ensure that $\boldsymbol{K}(\boldsymbol{X},\boldsymbol{X})$ is well-conditioned. The form of k is set to Radial Basis Function (RBF),

$$k(\boldsymbol{\xi}_i,\boldsymbol{\xi}_j) := \exp\left(-\frac{\|\boldsymbol{\xi}_i - \boldsymbol{\xi}_j\|^2}{2l_k^2}\right) \tag{25}$$

where l_k is the length scale hyperparameter associated with kernel k optimised during training to maximise log marginal likelihood of the form

$$\log \boldsymbol{p}(\boldsymbol{y}|\boldsymbol{X},l) := -\frac{1}{2}\boldsymbol{y}^\top\boldsymbol{K}_\sigma^{-1}\boldsymbol{y} - \frac{1}{2}\log|\boldsymbol{K}_\sigma| - c, \tag{26}$$

where $\boldsymbol{K}_\sigma = \boldsymbol{K} + \sigma_n^2\boldsymbol{I}$, $c = M/2\log 2\pi$ and $|\boldsymbol{K}|$ is determinant of $\boldsymbol{K}$. The RBF kernel was chosen since it corresponds to an infinite number of nonlinear transformations of the original input and consequently allows for a highly flexible model.

To construct an initial approximation as defined in (24), we first solve (21) over a randomly sampled reference input space $\boldsymbol{X}$, deriving optimal velocities for the subsequent time step and determining the value of l that best fits the solution set. During network simulation, for each vehicle (totalling N_v) in the simulation, the procedure to set the speed $v_i(t_n)$ for the ith vehicle at a time t_n involves the following steps. The model four-dimensional input $\boldsymbol{\xi}^*$ is extracted from the simulation, and the approximation (24) is used to predict the next time step's velocity, $\hat{v}_{t_n} = \hat{f}(\boldsymbol{\xi})$, along with the associated uncertainty, $\hat{\sigma} = \hat{\boldsymbol{\sigma}}(\boldsymbol{\xi}^*)$. It is important to note that $\hat{\boldsymbol{\sigma}}$ denotes the function generating predictions, while $\hat{\sigma}$ represents the prediction itself. If $\hat{\sigma}$ is below a predefined uncertainty threshold τ, the velocity for the next time step is set to $\hat{v}_{t_n}$. Conversely, if $\hat{\sigma}$ exceeds τ, the original optimal control problem (21) is resolved, and its solution, $v^*_{t_n}$, is used to update the velocity. Additionally, both the input $\boldsymbol{\xi}^*$ and the output $v^*_{t_n}$ are incorporated into the reference dataset. New parameters are then selected to maximise (26), facilitating the refinement of $\hat{\boldsymbol{f}}$ and $\hat{\boldsymbol{\sigma}}$ for subsequent vehicles and time steps. This methodology is detailed in Algorithm 1 and visually represented in Figure 3.

The value of l_k is recomputed periodically in order to take into account new data. It is noted that, if l_k is small, the model can overfit to $\boldsymbol{X}$ and $\boldsymbol{y}$. However, this situation is unlikely, since (26) contains a term, $\frac{1}{2}\log|\boldsymbol{K}_\sigma|$, which will more strongly penalise the small length scales as M increases [40]. Additionally, small values of l will result in high values of $\hat{\sigma}$ for any unseen data point, in which case (21) will be solved instead.

The velocity at a next time step obtained using (24) can be obtained at significantly lower computational cost than when (21) is used (especially if $[\boldsymbol{K}(\boldsymbol{X},\boldsymbol{X}) + \sigma_n^2\boldsymbol{I}]^{-1}$ is

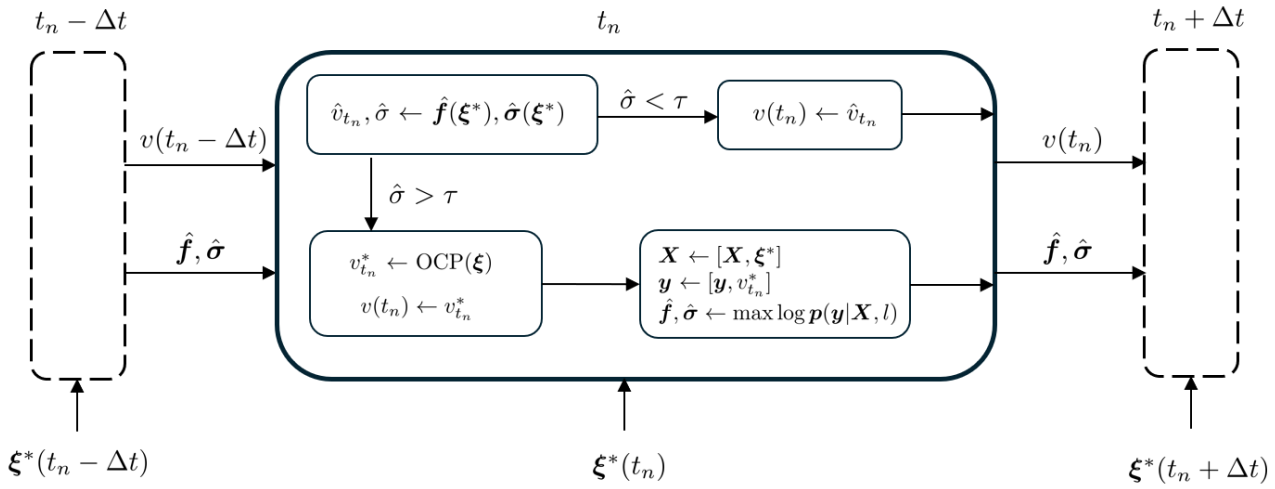

Fig. 3: This figure depicts a comprehensive workflow algorithm that integrates OCP and GPR within a network simulation for vehicle dynamics. For each vehicle, the algorithm retrieves current inputs and calculates the predicted output and its associated uncertainty, denoted as $\hat{\sigma}$. Based on the value of $\hat{\sigma}$ relative to a predetermined threshold τ, the algorithm either directly updates the velocity for the next time step or recalculates it using OCP to optimize driving efficiency. Throughout the simulation, the states of the vehicles, the decision outcomes, and the GPR model parameters are dynamically updated and stored in $\boldsymbol{X}$, $\boldsymbol{y}$ and $\hat{\boldsymbol{f}}$, respectively, ensuring a continuous refinement of the model's predictions and control strategies.

Algorithm 1 Algorithm workflow based on OCP and GPR

$\boldsymbol{X} \leftarrow$ SampleReferenceInputSpace()
$\boldsymbol{y} \leftarrow$ OCP($\boldsymbol{X}$) by solving (21) for each sample in $\boldsymbol{X}$
$\hat{\boldsymbol{f}}, \hat{\boldsymbol{\sigma}} \leftarrow \max \log \boldsymbol{p}(\boldsymbol{y}|\boldsymbol{X}, l)$
while NetworkSimulationIsRunning **do**
  for $i = 1$ to N_v **do**
    $\boldsymbol{\xi}^* \leftarrow$ GetInput()
    $\hat{v}_{t_n}, \hat{\sigma} \leftarrow \hat{\boldsymbol{f}}(\boldsymbol{\xi}^*), \hat{\boldsymbol{\sigma}}(\boldsymbol{\xi}^*)$
    if $\hat{\sigma} < \tau$ **then**
      $v_i(t_n) \leftarrow \hat{v}_{t_n}$
    else
      $v_{t_n}^* \leftarrow$ OCP($\boldsymbol{\xi}^*$)
      $v_i(t_n) \leftarrow v_{t_n}^*$
      $\boldsymbol{X} \leftarrow [\boldsymbol{X}, \boldsymbol{\xi}^*]$
      $\boldsymbol{y} \leftarrow [\boldsymbol{y}, v_{t_n}^*]$
      $\hat{\boldsymbol{f}}, \hat{\boldsymbol{\sigma}} \leftarrow \max \log \boldsymbol{p}(\boldsymbol{y}|\boldsymbol{X}, l)$
    end if
  end for
end while

precomputed). The computational time will depend on the size of $\boldsymbol{X}$, since (25) needs to be calculated between new sample $\boldsymbol{\xi}^*$ and every past observation constituting $\boldsymbol{X}$. On a standard laptop, for $M = 9000$ and a single new sample, the computation of (24) takes on average 0.002 s, while the solution of (21) takes on average 5.5s. In other words, even if (20) and (21) cannot be solved in real time, their approximation (24) can be utilised in real-life applications provided that the frequency of calculating (24) is greater than 0.002 s.

IV. Eco-driving evaluation methodology

In order to examine the effects of eco-vehicles on other car drivers, two types of impacts are introduced: *vehicle-induced* and *traffic-induced* influence. The vehicle-induced impact is defined as the driving style change of all vehicles following an eco-vehicle, in order to retain safe space gap and speed. For example, if the leader eco-vehicle is driving at substantially lower velocity and there is no opportunity for overtaking, all the following cars would need to reduce their speed as well. In this case, vehicles ahead of the eco-vehicle will not be affected by the presence of the eco-vehicle. Similarly, vehicles on road segments without eco-vehicles are not considered to be affected, since they do not modify their speed profile in response to eco-vehicles in the close vicinity. The traffic-induced influence is defined as the driving style change of road users due to traffic condition change caused by the presence of eco-vehicles. An example is a congestion created when eco-vehicles are forced to drive at slower velocities. The congestion can spread throughout the network, affecting network participants which are at different locations in the network, often considerable distance away from eco-vehicles. This can have negative effects on energy consumption of conventional vehicles, for example, through stop-and-go waves where repeated acceleration and deceleration lead to negative environmental impacts.

In order to examine both vehicle-induced and traffic-induced impacts of eco-vehicles, two scenarios are created:

1) **A platoon** where n conventional vehicles follow an eco-vehicle, and they are not allowed to overtake is considered as the first case study (see Figures 5). This scenario has been well-established in the literature, in [41] and [42]. In our study, it is employed primarily as an initial validation test case before progressing to

more intricate scenarios. It allows assessing the vehicle-induced impact of an eco-vehicle on the following vehicles. It is assumed that the eco-vehicle responds to a car ahead of it, knowing its full speed profile. For this analysis, the speed profile used for validation was collected in real-life setting and corresponds to a behaviour of a real driver (it will be referred to as "Real vehicle"). The upper limit on the energy efficiency that can be passed onto conventional vehicles is investigated here. The problem formulation and results corresponding to this case are given in Section V. In this scenario only a single eco-vehicle exists and running a full OCP optimisation does not involve high computational cost. Hence, a methodology outlined in Section III-C is employed here.

2) **An urban network** in the Selly Oak area (Birmingham, UK) is considered as the second case study to investigate both vehicle-induced and traffic-induced impacts of eco-vehicles. Different proportions of eco-vehicles (ranging between 5% to 50%) are introduced into the network for *low-density traffic* and *high-density traffic* cases, and their effect on conventional vehicles is examined. The problem formulation and results corresponding to this case are given in Section VI. Since for large proportions of eco-vehicles the computations cost associated with running multiple OCP optimisations becomes prohibitive, the approximation of (21) introduced in Section III-D using GPR is employed instead.

In order to take into account heterogeneity of network participants, a model describing variability of individual agents is required. A realistic formulation is highly complex since each car should be characterised by distinct specifications, and even for the same type of vehicle, each driver should be defined with a unique driving style which cannot be easily expressed using few parameters. In this study, it is assumed that the network consists of five vehicle types: car, motorcycle, Light Goods Vehicle (LGV), Heavy Goods Vehicle (HGV) and bus, with different power consumption characteristics. The eco-vehicles are assumed to be of the car type with one engine model in order to reduce the computational complexity. With assuming a single engine model for the eco-vehicles, the eco-driving optimisation is significantly simplified using the proposed GPR (see Section III-D). The power maps used for other types of vehicles are also constant for the same type and are obtained by scaling acceleration and velocities but retaining the shape and magnitude visible in Figure 2. The scaling factors are chosen such that maximum acceleration and deceleration of various vehicles (see Table II) and speed of $25\ \mathrm{m/s}$ (corresponding to maximum speed limit in the urban road network) are retained in the modified power map. It is also considered that the peak vehicle efficiency is approximately 0.9 for vehicle masses showed in Table II. The battery power maps for motorcycle, LGV, HGV and bus are depicted in Figure 4.

It is assumed that driver behaviour is deterministic, i.e. not subject to random perturbations in their dynamics. The driving

TABLE II: IDM driving style parameters used in the urban network simulation.

	Car	Motorcycle	LGV	HGV	Bus
$a_{\max}$ (m/s^2)	2.5	5.0	2.0	1.3	1.0
b (m/s^2)	4.5	9.0	4.0	3.5	3.5
l (m)	4.3	2.2	6.5	7.1	12.0
mass (t)	1.5	0.26	2.3	7.5	12.0
Probability distribution*	0.827	0.030	0.123	0.016	0.004

* Based on the VEH0104 dataset [43]

style of conventional drivers is given by IDM dynamics [38]:

$$\dot{v}_i = a_{\max}\left(1 - \left(\frac{v_i}{v_d}\right)^4 - \left(\frac{s^*\left(v_i, \Delta v_i\right)}{s_i}\right)^2\right) \quad \text{with } s^*\left(v_i, \Delta v_i\right) = s_0 + v_i t_0 + \frac{v_i \Delta v_i}{2\sqrt{a_{\max} b}} \tag{27}$$

where b is comfortable breaking deceleration, $s_0 = 2.5$ is the minimum space gap, $t_0 = 1.5$ is the safe time headway, and $\Delta v_i = v_i - v_{i-1}$. The value of v_d is set dynamically to v_{max}, which is the maximum allowed speed on a road segment. Similar to DSM in (8), the IDM can be described using five constant parameters:

$$S_{IDM} = \left(v_d, a_{max}, b, t_0, s_0\right), \tag{28}$$

which have equivalent interpretation apart from b.

In order to imitate a variety of realistic driving styles, we considered IDM parameters to be variable within the population of drivers. For simplicity, it is also assumed that all parameters follow the Gaussian distribution expressed by $\kappa \sim \mathcal{N}(\bar{\kappa}, 0.15\bar{\kappa})$, where $\bar{\kappa}$ is a mean value of κ. The mean parameter values are given in Table II. The likelihood of a vehicle being of a particular type is defined as "Probability" in Table II. In the platoon test case, all vehicles are assumed to be of the "Car" type, whilst all five different types of vehicles showed in Table II are present in the urban network test case,

Many existing microscopic traffic simulators specify uncorrelated marginal distributions for each parameter in IDM, represented by mean and standard deviation [44]. The correlation between IDM parameters was investigated in [44] and [45] based on numerical fits to different drivers in NGSIM trajectory data. In both cases, the correlation values were smaller than 0.3. Nonetheless, despite a similar approach, the corresponding entries in the correlation matrix varied considerably. For example, in [44] the correlation between s_d and v_d is reported to be 0.248 whilst in [45] this values is equal to 0.051. Another example involves correlation between a_{max} and b, which was reported to be 0.124 and 0.304 in [44] and [45] respectively. The insight into reasons behind such disparities are given in [46], where it is demonstrated that the results are very sensitive to the choice of a fitting algorithm and in many cases the fit did not converge to true values. It is noted that the analysis was based on NGSIM data, which contains velocity profiles in a highway environment. It is possible that similar investigation based on data collected in urban environment can give stronger correlation between IDM parameters, but there is no study which allows a definite conclusion to be made. Taking into account the relatively small correlation between

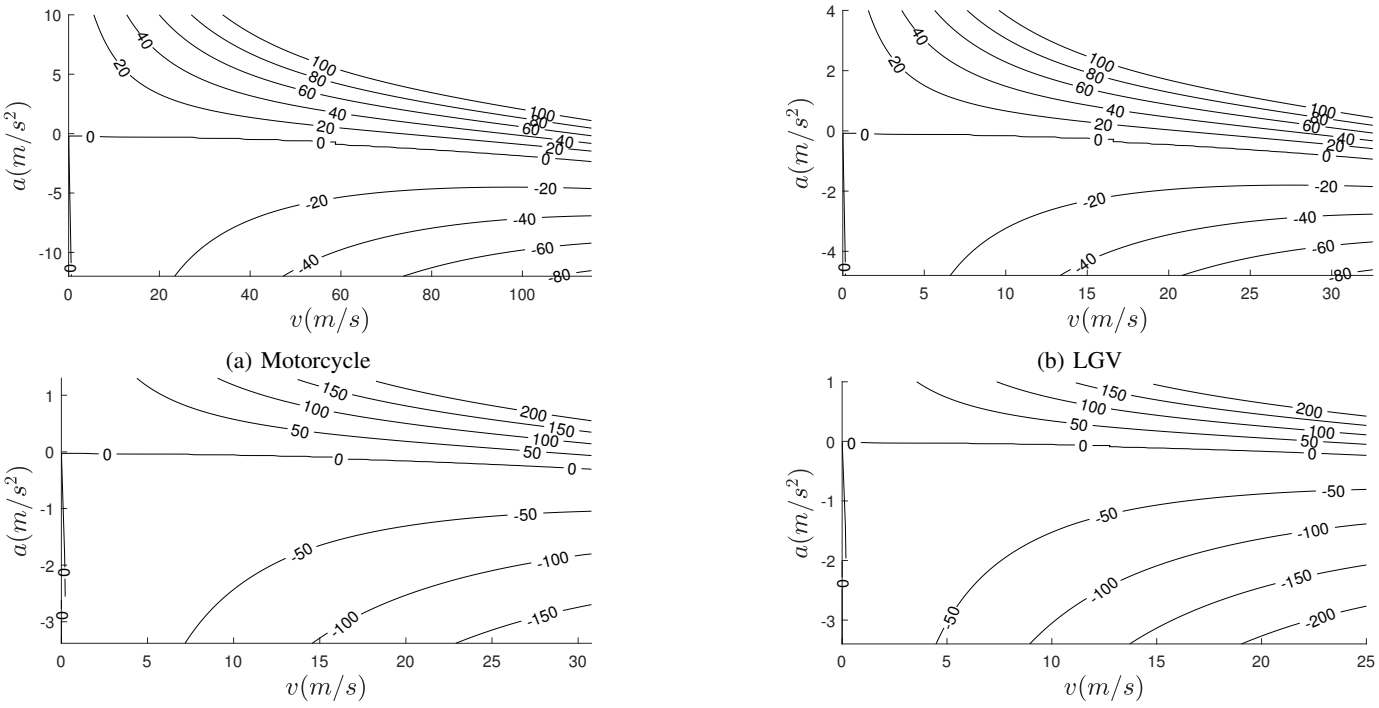

(a) Motorcycle

(b) LGV

(c) HGV

(d) Bus

Fig. 4: Battery power, P_b, for different types of conventional vehicles present in an urban network scenario.

IDM parameters in [44], [45] and considering the lack of consensus on the correct correlation coefficients and imitating approaches used in some microscopic traffic models, in this study it is assumed that the IDM parameters are uncorrelated. Furthermore, the parameters in (4) with similar interpretation to IDM, are assigned the mean values $\bar{k}$.

V. Case Study: Platoon of Cars

A. Case study design

The platoon scenario presented in Figure 5 is used to examine the vehicle-induced effects of eco-driving on other road users. To establish a baseline for comparison, the speed profiles of two vehicles, the leader and the eco-vehicle, were recorded in a real-life setting. The speed profile of the eco-vehicle was recorded with an On-Board Diagnostics sensor. This vehicle is referred to as the "Real Vehicle" in Figure 5. The speed profile and headway of the leader vehicle were recorded using the Automobile Data Acquisition Module [47]. This vehicle is referred to as the "Platoon Leader" in Figure 5.

It is assumed that the optimised drivers follow the vehicle exhibiting the conventional driving style demonstrated by the "Platoon Leader". In this analysis, this is characterised by replacing the speed profile of the "Real Vehicle" with one of the optimised profiles. Three eco-driving strategies introduced in Section III-C, NATURAL, BALANCED and ECO, are simulated to respond to the platoon leader. The energy consumption of a "Real Vehicle" will be used as benchmark for comparison. Since the platoon leader's velocity is known for the whole trip duration, optimisation has been carried out according to (20), rather than with the receding horizon approach in (21). Additionally, the speed measurement of the

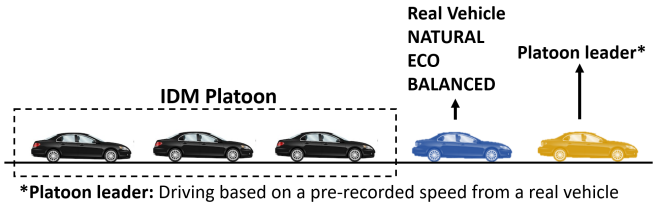

Fig. 5: Schematic representation of the simulation setup used in Section V.

follower car are also recorded, in order to compare eco-driving strategies with a response of a human. The Real vehicle/Eco-vehicle in Figure 5 is followed by $i = 1, 2, ...n$ conventional vehicles governed by IDM dynamics (see Section IV). All vehicles are assumed to be of the "Car" type here (see Table II).

The conventional vehicles are entering the scenario at uniform intervals and speeds, i.e. every 8 s at a speed of 15 m/s. The duration of the simulation is set to 700 s, which is the travel time of the reference real-vehicle. With a constant inflow of 7.5 vehicles/min, in total 87 vehicles (85 conventional vehicles) are able to enter the scenario within this travel time. The energy consumption of each vehicle in the platoon is computed by introducing the i-th speed and acceleration profile $v_i(t)$ and $a_i(t)$ and using (22).

In order to obtain statistical information about reduction in power consumption which takes into account different type of drivers, a hundred unique simulations are created, with the only difference between them being IDM parameters assigned to conventional driver. Among them, every simulation is

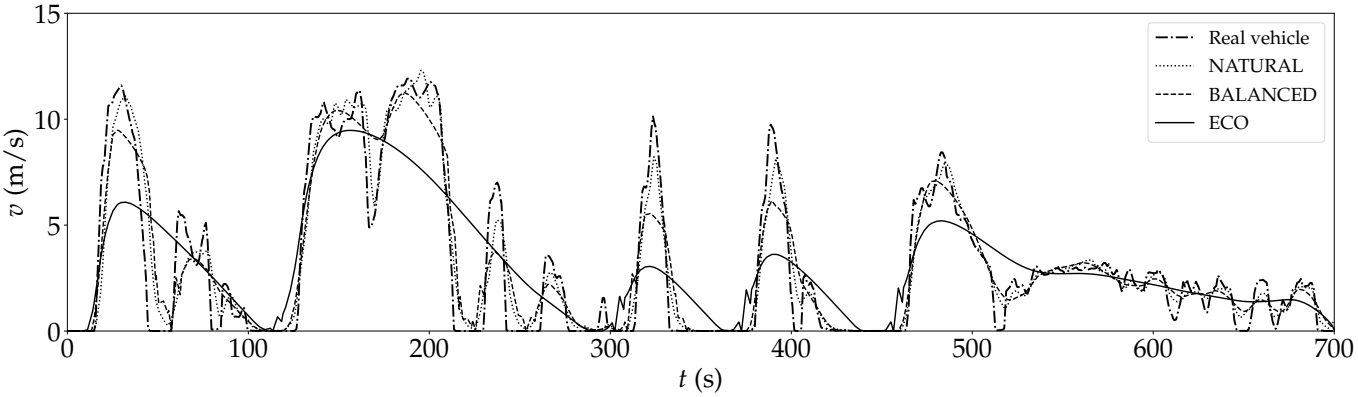

Fig. 6: The eco-driving speed profiles together with speed profile of a real driver. The speed profile corresponding to "Real vehicle" was collected in a real driving setting, whilst all the other profiles are obtained through OCP optimisation.

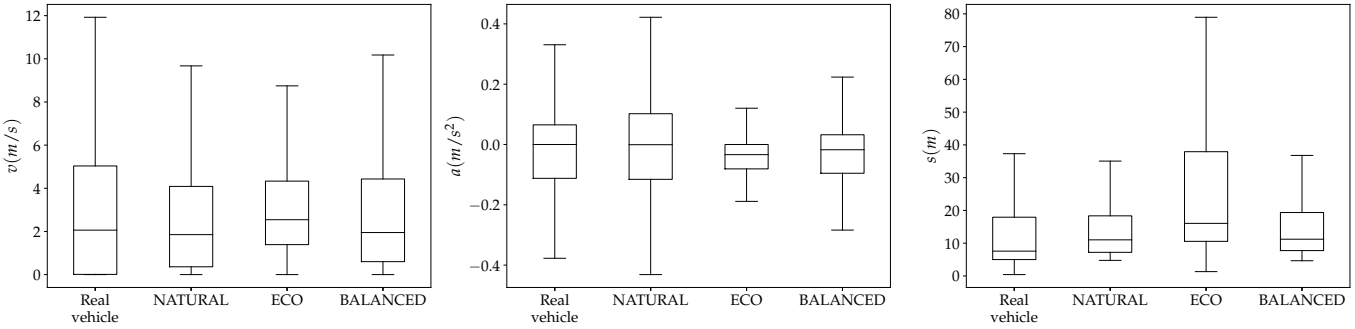

Fig. 7: Statistical characteristics corresponding to speed profiles showed in Figure 6.

conducted for all the speed profiles explained in Section III-C and showed in Figure 6, in total producing 300 sets of results involving eco-vehicles. The v_{max} on the travelled road, and consequently v_d, is set to 15 m/s.

B. Results and discussions

The speed profiles obtained using three eco-driving strategies together with a response of a real vehicle are shown in Figure 6. The statistical properties of each of the speed profiles are shown in Figure 7. It can be seen that the solutions for ECO and BALANCED give smoother velocity profiles characterised by lower values of $|a|$ compared to the real vehicle. The ECO case shows conventional characteristics of the eco-driving style, i.e. large acceleration until a maximum allowed velocity is reached followed by coasting behaviour. Such a behaviour results in a large space gap which in a real-life scenario is likely to negate any positive effect on the following vehicles, since vehicles will be able to overtake slow-driving eco-vehicles. For example, it is shown in Figure 7 that in the analysed case, the space gap in the ECO driving style reached values of 80 m, which is sufficiently large to allow for overtaking manoeuvres. The coasting behaviour in ECO is exhibited by larger mean speed than for other strategies, since eco-vehicle remains stationary for a shorter amount of time. The maximum speed of all eco-vehicles is observed to be smaller than for the real-driver, which will also contribute to energy savings, since vehicles will not be required to overcome larger aerodynamic drag.

TABLE III: Energy consumption E and relative energy improvement ΔE corresponding to speed profiles in Figure 6.

	Real vehicle	NATURAL	ECO	BALANCED
$E\ \left(\frac{kWh}{100km}\right)$	5.44	5.09	4.29	4.75
$\Delta E\ (\%)$	–	6.4	21.1	12.7

Table III shows the total energy consumption E and relative energy improvement ΔE corresponding to speed profiles in Figure 6. The relative improvements in energy consumption of each conventional ego-vehicle ΔE (23), where larger values of ΔE correspond to larger energy savings, are presented in Figure 8. A clear positive effect can be seen in Table III and Figure 8 as all three simulated driving styles result in less energy consumption and smaller acceleration/deceleration compared to the real vehicle. The amount of reduction follows the expected pattern, i.e. the largest reduction is obtained for ECO (4.29 kWh/100km) whilst the lowest is observed for NATURAL (5.09 kWh/100km). As shown in Figure 8, the beneficial impact extends to multiple vehicles and reduces as the distance from the leading eco-vehicle increases. For instance, in the case of a BALANCED leader, energy savings are greater than 10% for the 11^{th} follower (see Figure 8). In

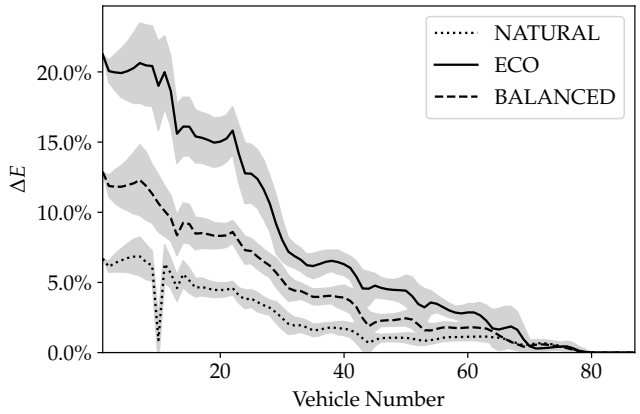

Fig. 8: The mean energy savings of all ego-vehicles in the platoon. The filled area corresponds to values within one standard deviation away from the mean.

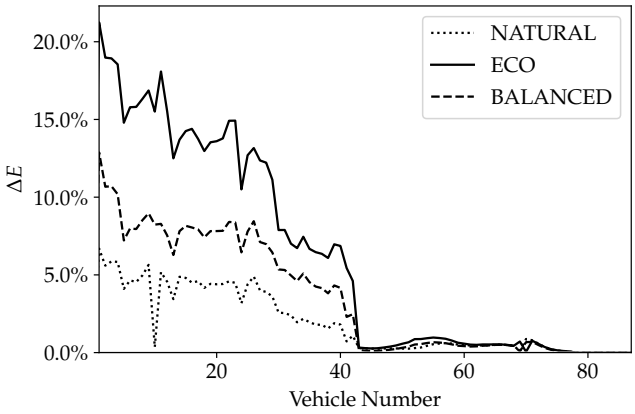

Fig. 9: Energy savings of the simulations with the smallest energy reductions.

the case of an ECO leader, the energy savings are greater than 10% even for the 28^{th} follower.

In a similar analysis presented in [35], a reduction in energy consumption of 35% is achieved when the first vehicle in a platoon follows the eco-driving strategy. It should be noted that the test scenario used in [35] differs considerably to the one used here. In [35], the primary objective was to avoid stopping at traffic lights and, unlike here, the eco-vehicle was not constrained by a leading vehicle, which allows for more freedom to choose an optimal velocity profile. Additionally, the test case in [35] was characterised by larger maximum velocity, so that when stopping is avoided, the longer periods of acceleration are reduced, leading to more significant differences.

As explained in Section IV, the presence of random variable κ allowed the identification of scenarios with the largest and smallest energy reduction. The greatest improvements are observed, when the ego-vehicles are on average characterised by lower values of a_{max}, which corresponds to drivers with eco-driving tendencies, favouring smooth acceleration and deceleration. One of the simulations where the energy reduction was smallest is presented in Figure 9. A significant drop in energy reduction is visible for the 43^{th} follower in the platoon. Examining the parameters characterising its behaviour, a significantly lower value of desired free-flow velocity v_d is observed. A slow driving style of this vehicle put an upper bound on speed in the eco-driving profiles, limiting the magnitude of a nudging effect. Similar observation can be made for other simulations with small total energy reduction. It can be concluded that the positive impact on energy minimisation is retained, as long as vehicles associated with abnormally small values of v_d are not present in the platoon.

VI. Case study: road network with different vehicles

A. Case study design

A test case based on a real urban network in the Selly Oak area (Birmingham, UK) is developed (see Figure 10). The area is $8.26\ \mathrm{km}^2$ with 552 routes and 12 traffic lights located along the main roads. The total length of all lanes in this case study is $41.2\ \mathrm{km}$. The primary reason for the choice of Birmingham is public availability of real-time traffic flow data from induction loops, allowing for realistic modelling of trip and route distributions so that real-life traffic characteristics are reproduced in the simulation. In addition, Selly Oak contains the highest percentage of active induction loops (64 induction loops covering the area) and is characterised by high traffic volumes, due to the presence of large residential area and places of interest such as University of Birmingham and a hospital. Hence, the effects of eco-driving can be explored.

The location of traffic signals along the road network is shown in Figure 10. The model of the network is created by using OpenStreetMap data and the real-time traffic data from the Birmingham and West Midlands traffic data portal (https://data.birmingham.gov.uk/dataset/wm-utmc).

Traffic demand is modelled with the Four-Step Model [48], which consists of trip generation, trip distribution, mode choice and route choice. For trip generation, the utilisation frequency of each origin and destination point is estimated using the flow data. The trips are distributed via an Origin-Destination (O-D) matrix, where initial traffic assignment is performed using a technique proposed in [49].

Initial trip assignment within the matrix typically necessitates calibration to address discrepancies in the estimated trip distributions. This calibration employs the Furness method, which adjusts the trip matrix iteratively. The adjustment process utilises the formula $\boldsymbol{T}_{ij,\text{new}} = \boldsymbol{a}_i \boldsymbol{b}_j \boldsymbol{T}_{ij,\text{old}}$, with $\boldsymbol{a}_i$ representing the vector of origin growth-factors, and $\boldsymbol{b}_j$ the vector of destination growth-factors. These factors are calibrated against specified target vectors for origin $\boldsymbol{O}_{i,\text{target}}$ and destination $\boldsymbol{D}_{j,\text{target}}$, aiming to satisfy the equality $\sum \boldsymbol{O}_{i,\text{target}} = \sum \boldsymbol{D}_{j,\text{target}} = \boldsymbol{T}_{\text{total,target}}$. More specifically, this process in-

volves the following steps to adjust and validate the trip matrix:

- Begin by setting all $\boldsymbol{b}_j$ values to 1.
- Calculate the origin growth factors, $\boldsymbol{a}_i$, to ensure they align with the predefined target origin criteria, $\boldsymbol{O}_{i,\text{target}}$.
- With $\boldsymbol{a}_i$ determined, compute the destination growth factors, $\boldsymbol{b}_j$, to meet the target destination criteria, $\boldsymbol{D}_{j,\text{target}}$.
- Repeat the calculation of $\boldsymbol{a}_i$ and $\boldsymbol{b}_j$ until the convergence criteria of the system are satisfied.

Model calibration and validation utilise the GEH statistic [50], expressed as

$$\text{GEH} = \sqrt{\frac{2(V_{\text{sim}} - V_{\text{obs}})^2}{V_{\text{sim}} + V_{\text{obs}}}}, \tag{29}$$

comparing simulated V_{sim} and observed V_{obs} traffic volumes. For the simulation to be indicative of actual traffic, it is recommended that the GEH statistic should remain below 5% in excess of 85% of cases. In the present study, the iterative calibration procedure was deemed convergent when the GEH statistic alterations between successive iterations were under 0.5%, ensuring that the adjusted traffic flows fell within the acceptable range of accuracy and thus confirming the model's efficacy in depicting real traffic conditions.

TABLE IV: Calibration Notation

Variable	Explanation
$\boldsymbol{T}_{ij}$	Number of trips per hour between origin i and j
$\boldsymbol{O}_{i,\text{target}}$	Target number of trips originating from i
$\boldsymbol{D}_{j,\text{target}}$	Target number of trips arriving at desitnation j
$\boldsymbol{T}_{\text{total, target}}$	Target total number of trips
$\boldsymbol{a}_j$	Vector of origin growth factors
$\boldsymbol{b}_j$	Vector of destination growth factors
GEH	GEH-statistic
V_{sim}	Simulated traffic volume
V_{sim}	Observed traffic volume

A percentage of vehicles between 5% and 50% is set to follow the proposed eco-driving methodology in Section IV, while the rest of drivers are travelling based on the IDM. In order to assign a mode of transportation to each trip, VEH0104 dataset [43] is used, which provides the distribution of different vehicle types in different UK regions. Corresponding probability distributions are shown in Table II. Considering the O-D matrix, it is assumed that drivers choose the shortest path to their destination based on Dijkstra's algorithm [51]. More information about the construction of this test case can be found in [52].

For the simulation of the urban scenario, the GPR outlined in Section III-D is utilised. Contrary to the platoon scenario in Section V-A, the assumption of having full knowledge about the leader speed profile is not viable in the urban network scenario. The speed of the lead vehicle changes at every time-step ($\Delta t = 0.1s$) in response to optimised velocity profiles of eco-vehicles in the network. This makes some of the previously obtained OCP solutions not valid, and in those cases the receding horizon problem in (21) is solved instead. The computational cost of repeatedly solving (21) for multiple vehicles is unavoidable. Furthermore, the uncertainly threshold

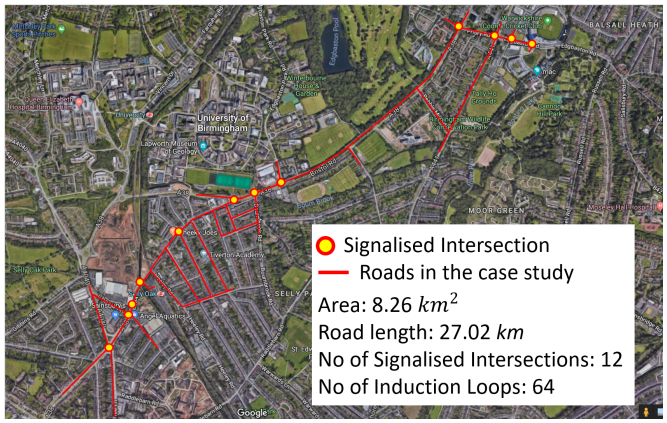

Fig. 10: Map of the simulated road network of Selly Oak (Birmingham, UK)

τ is set to 0.01 and (21) is solved only for $\tau > 0.01$ (see Section III-D).

The traffic lights in the simulation and proposed optimisation are approached in the following manner. It is assumed that vehicles do not possess V2V or V2I communication capabilities. As a result, drivers can only perceive the current traffic light stage. This assumption accurately replicates the driver's perception and current autonomous systems, which rely on vision-based algorithms for traffic state detection [13], [53]. Furthermore, due to concerns surrounding the privacy and reliability of V2V and V2I communications [12], it is improbable that these technologies will be introduced in the immediate future.

In order to solve (21), traffic lights are treated as a leader vehicle positioned at the end of the lane with speed v_{i-1}, which is dependent on the traffic light stage, so that configurations where an eco-vehicle does not have a leader and is approaching a signalised intersection are considered. During the red light, $v_{i-1} = 0$, whilst during the green light $v_{i-1} = v_{max}$. In both cases s is set to $s_{junction} = l_l - x_i$, where l_l is the length of the lane and x_i is the position of the eco-vehicle along the lane.

Two safety mechanisms are incorporated to avoid collisions:

1) A precise value of s is obtained by looking for a leader vehicle not only on the current lane but also on the subsequent lanes along the vehicle's route. The search stops when a lead vehicle or a traffic light is found, or the maximum space gap of $s_{max} = 250$ m is reached. If $s = s_{max}$, then v_{i-1} is set to v_{max};
2) When the velocity v_i is less than 0.1 m/s and the space gap is $s \leq s_0$, the predicted velocity $\hat{v}_{t_n+\Delta t}$ is set to zero. This safety mechanism is introduced to avoid collisions at road junctions which can lead to vehicle movements when they are expected to remain stationary.

Two different streams with low-density traffic and high-density traffic are analysed. The analysis employed traffic data from inductive loop detectors, captured during 2016 and 2017. This period was chosen for its consistent data availability before the onset of significant disruptions caused by construction activities in 2018. Our study focused on average weekday traf-

fic conditions, deliberately excluding weekend data to avoid skewing results with atypically low traffic flow peaks observed during these periods. Traffic data were aggregated into 15-minute intervals, extended from the original 5-minute intervals to normalise time intervals between detectors and compensate for any discrepancies due to unsynchronised clocks, typically off by about one second. Traffic volumes were categorised as follows: 1) low-density traffic was calculated as the average traffic flow from weekdays, providing a baseline for normal conditions; whilst 2) high-density traffic was defined as conditions where traffic flow exceeds the mean by 20%. This threshold was determined empirically, identifying when traffic begins to deviate substantially from normal and lead to congestion.

In low-density traffic, the average number of vehicles in the simulation is 161 with maximum traffic density of 0.28 vehicle/km on a single lane. The total distance travelled by all vehicles is 106 km in half an hour. The average distance between vehicles is expected to be larger in low-density traffic and therefore in many cases the vehicle do not require imitating the velocity profile of the leading vehicle to retain a safe distance. At the same time, there is an increase in freedom to choose a velocity profile which provides the largest reduction in vehicle power consumption. Consequently, the effect of eco-driving on other vehicles can be assessed.

In high-density traffic, the average number of vehicles in the simulation is 561 with maximum traffic density of 0.37 vehicle/km on a single lane. The total distance driven by all vehicles is 2008 km. The high-density traffic allows investigating traffic conditions at "peak" hours when there is significant congestion in the network. Hence, the available solutions are reduced in this case (due to smaller space gap) but drivers are more likely to imitate the behaviour of the eco-vehicle ahead in order to retain a safe space gap.

Separate simulations are performed for the different percentages of eco-vehicles at the initialisation time-steps: 5%, 10%, 15%, 25% and 50%. Similar to Section V, each simulation is repeated for three scenarios for different eco-vehicle strategies: NATURAL, ECO and BALANCED. In each case, a simulation is conducted over 30 min.

Network generation and traffic simulation were performed using the Simulation of Urban MObility (SUMO) platform, with configuration details derived from the SellyOak traffic model. These details are accessible via GitHub repository [54]. The Optimal Control Problem (OCP) was formulated and resolved using GPOPS-II within MATLAB, while Gaussian Process (GP) modelling was conducted using the scikit-learn library in Python. The integrative code linking SUMO simulations with MATLAB for OCP and Python for GP modelling is available on GitHub [55]. This repository includes both the final GP model and the MATLAB scripts necessary for OCP optimisation.

Please be aware that replicating the simulations may result in variations from the reported results, primarily due to stochastic elements in our methodology. These include the initial random sampling from uniform distributions, which may not fully represent the input space, potentially affecting the initial state of the GP model. Additionally, the random uniform selection of vehicles for the eco-driving strategy contributes to the variability in simulation outcomes.

Since the simulation is stopped after a fixed period of time, vehicles' travel distance varies. In order to make a fair comparison, the energy usage per distance travelled is computed as:

$$E_n = \frac{\sum_{i=1}^{N} E_i}{\sum_{i=1}^{N} x_i(t_f)}. \tag{30}$$

In Table V, the energy usage is split to values corresponding only to conventional vehicles (IDM based vehicles) and eco-vehicles. The relative improvement is defined in reference to the energy usage $E_{n,ref}$ where only IDM vehicles are present in the network, as shown in (31).

$$\Delta E_n = \frac{E_{n,ref} - E_n}{E_{n,ref}} \tag{31}$$

In order to investigate the impact of the proposed eco-driving strategies on travel time, Pearson's correlation coefficient ρ is calculated in (32) for two variables of travel time and energy consumption. Since the simulations are terminated for $t > 30$ min, the travelled distance of two vehicles are not necessarily the same. Those differences, if not accounted for, can misrepresent change in travel time, therefore, the concept of *common travelled distance* is introduced, which corresponds to the smaller travel distance between two trips that are being compared. Consequently, Pearson's correlation coefficient ρ is calculated as:

$$\rho = \frac{\mathrm{Cov}(\Delta(t_x)_i, E_i - E_{i,ref})}{\sigma_{\Delta(t_x)_i}\sigma_{E_i - E_{i,ref}}}, \tag{32}$$

Travel time required to drive the common travelled distance x is defined as t_x. $\Delta(t_x)_i = (t_x)_i - (t_x)_{i,ref}$ is the difference between travel time of a vehicle i, which corresponds to a simulation with eco-vehicles, and a vehicle i, ref, which corresponds to a simulation only with IDM vehicles, to drive a common travel distance x. $E_i - E_{i,ref}$ represents the absolute change in energy consumption. Sample standard deviations of variables $\Delta(t_x)_i$ and $E_i - E_{i,ref}$ are presented by $\sigma_{\Delta(t_x)_i}$ and $\sigma_{E_i - E_{i,ref}}$ respectively.

B. Results and discussions

The relative improvements in energy consumption of eco-vehicles and conventional cars in low-density traffic are presented in Table V. Energy consumption improvement of up to 0.8% and 14.6% are obtained for conventional and eco-vehicles respectively. For eco-vehicles, ECO displays the largest reduction in the energy consumption in comparison to NATURAL and BALANCED which is expected. Also, despite smaller emphasis on fuel consumption in NATURAL, the first NATURAL results in higher energy savings in comparison to BALANCED in few situations (e.g. 10% eco-vehicles). This is due to the fact that the optimisation problem in (21) is solved for a short prediction horizon of 60 s and does not take into account long-term impact of traffic lights along the travelled route.

An example of the impact of traffic lights on energy consumption is presented in Figure 11. An eco-vehicle is

TABLE V: Relative improvements in energy consumption in **low-density traffic** considering different ratios of eco-vehicles in the case study.

	Ratio of Eco-vehicles in the network				
Eco-vehicle type	5%	10%	15%	25%	50%
	ΔE_n (31) for **conventional vehicles** (IDM based)				
NATURAL	0.0%	0.1%	0.2%	0.2%	0.7%
ECO	0.2%	0.5%	-0.3%	0.2%	0.0%
BALANCED	0.4%	0.4%	0.6%	**0.8%**	0.1%
	ΔE (31) for **eco-vehicles**				
NATURAL	8.5%	7.0%	7.6%	6.3%	8.5%
ECO	7.5%	14.4%	11.3%	**14.6%**	12.8%
BALANCED	6.2%	4.5%	9.9%	7.1%	8.3%

TABLE VI: Relative improvements in energy consumption in **high-density traffic** considering different ratios of eco-vehicles in the case study.

	Ratio of Eco-vehicles in the network				
Eco-vehicle type	5%	10%	15%	25%	50%
	ΔE_n (31) for **conventional vehicles** (IDM based)				
NATURAL	0.0%	0.4%	0.8%	2.2%	0.3%
ECO	1.2%	2.2 %	4.6%	**5.1%**	1.6%
BALANCED	2.7%	3.0%	2.7%	2.3%	3.2%
	ΔE (31) for **eco-vehicles**				
NATURAL	10.1%	10.6%	10.1%	14.1%	14.0%
ECO	17.2%	16.7%	17.3%	22.7%	19.3%
BALANCED	15.1%	14.9%	11.8%	14.5%	**22.7%**

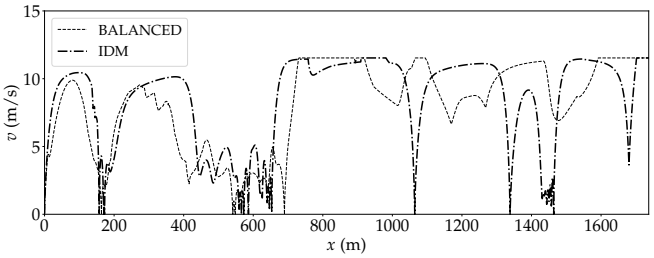

Fig. 11: An example where the difference in energy consumption comes not from the velocity profile, but primarily from not taking into account traffic lights.

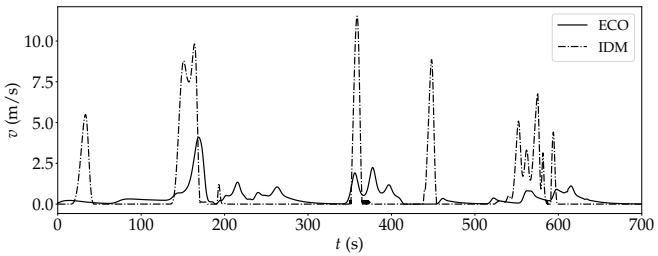

(a) ECO ($\Delta E > 0.2$)

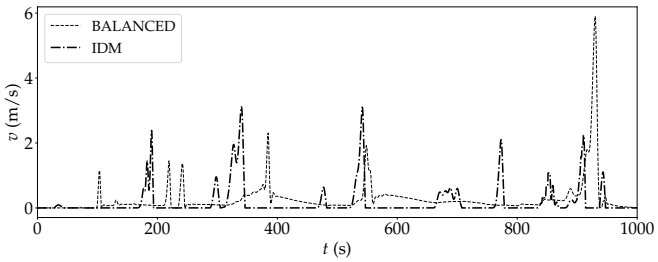

(b) BALANCED ($\Delta E > 0.2$)

Fig. 12: Examples of velocity profiles of conventional vehicles when either all vehicles follow IDM or when 15% of vehicles follow an eco-driving style.

able to drive through the traffic junction without a significant reduction of velocity at $x \approx 1100$ m. Due to slight variation of the velocity profile, a conventional vehicle is not able to pass through the junction within the same traffic light cycle and needs to stop. This results in a knock-off effect for $x > 1200$ m, where the vehicle is required to slow down and accelerate back to the desired speed multiple times. It also results in energy consumption increase. These types of events are prevalent for all vehicles including eco-vehicles, and they are in fact expected, due to formulation of (21), where traffic light cycles are not incorporated into the optimisation and only a short prediction horizon is taken into account. Hence, the total reduction in energy consumption of all types of vehicles are analysed here.

The energy consumption improvements for different percentages of eco-vehicles in the simulation in high-density traffic are shown in Table VI. Energy consumption improvement of up to 5.1% and 22.7% are gained for conventional and eco-vehicles respectively. The reasons could be: 1) in high-density traffic, space gap between vehicles is smaller and vehicles are forced to imitate the behaviour of the leading eco-driver; 2) speed variability is less in congestion which leads to smaller discrepancies between travelled distances and to reduced impact from the presence of traffic lights as shown in Figure 12.

For high-density traffic scenario, ΔE stays on average constant for different percentages of eco-vehicles in the network. It is notable that even for 5% penetration rate, there is a positive effect on conventional vehicles. The results for a platoon scenario in Figure 8 demonstrates that for traffic density close to road capacity, the effect of a single eco-vehicle can propagate even to vehicles which are considerably far away. This type of high density situations are intermittent in high-density traffic, hence a single eco-vehicle can have an impact on many other network participants. In addition, in a low-density traffic, despite conventional vehicles experiencing negligible reduction in energy consumption, the overall effect is still positive, if both types of vehicles are accounted for.

Figure 13 shows the histograms of ΔE for conventional vehicles corresponding to high-density traffic and when 15% of vehicles follow an eco-driving strategy. Positive and negative energy consumption changes can be seen due to traffic lights' impact, Nonetheless, the distribution is significantly skewed towards the positive values for ECO, the skewness is reduced for BALANCED and symmetry is approximately restored for NATURAL.

A few chosen examples of velocity profiles are shown in Figure 12. In Figure 12(a), a vehicle which responds to

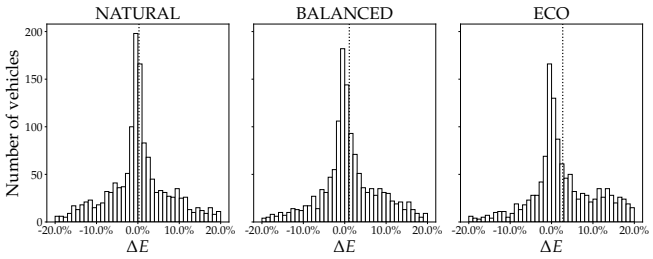

Fig. 13: Relative energy consumption improvements when 15% of vehicles follow eco-driving strategies. The dashed lines show the mean value of ΔE.

the eco-vehicles following the ECO strategy is compared with a scenario where every car's dynamics is governed by IDM. It can be seen that a conventional vehicle imitates the behaviour of a leading eco-driver (e.g. gentler acceleration/ deceleration, smaller instantaneous velocity). When there is no eco-vehicle present in the simulation, the speed profiles are primarily characterised by large acceleration to reach the speed limit, followed by sharp breaking. Figure 12(b) shows the velocity profile of a vehicle responding to eco-vehicles driving according to the BALANCED approach. Here, conventional vehicle exhibits a mixture of different styles, where both, sharp acceleration and deceleration representing akin to IDM style, and slow approach to a junction similar to eco-driving are present. The profile showed in Figure 12(b) is more natural and results in higher acceptance than the one showed in Figure 12(a).

The velocity profiles with negative reduction in energy consumption in Figure 13 are similar to the behaviour presented in Figure 11, i.e. the vehicle responding to the eco-vehicle ahead is forced to repeatedly accelerate and decelerate due to not passing through the junction within a specific traffic stage.

As mentioned in Section IV, a high number of proposed eco-driving strategies in the literature are based on imposing a maximum bound on acceleration and deceleration [30], [31], [32] which leads to smaller mean speed and higher travel time. The impact of eco-driving on travel time in high-density traffic with 15% eco-vehicles is investigated in this study by looking at mean speed $\bar{v}$ and correlation coefficient ρ (32). The results are presented in Table VII. It can be seen that $\bar{v}$ decreases when vehicles follow ECO or BALANCED strategy. The difference is only 0.02 $\mathrm{m/s}$ though, which is an acceptable trade-off for the achieved reduction in energy consumption. Notably, $\bar{v}$ increases for NATURAL. The higher values of ρ demonstrate that greater reduction in energy consumption of a vehicle is likely to increase its travel time. Nonetheless, the correlation is small, with the largest magnitude of 0.34 observed for ECO. Similar conclusions can be reached for remaining simulations with different percentages of eco-vehicles, therefore, presentation of the corresponding statistics is omitted. No significant differences in values of $\bar{v}$ for conventional vehicles are observed in low-density traffic scenario.

TABLE VII: Mean speed of conventional vehicles and the correlation coefficient between travel time and energy consumption, ρ in (32), in high-density traffic with 15% eco-vehicles.

	NATURAL	ECO	BALANCED	IDM
$\bar{v}$ (m/s)	3.63	3.44	3.55	3.57
ρ	0.19	0.34	0.28	-

VII. Conclusions and Future Work

We show that in the presence of eco-vehicles following the strategy introduced in [37], the reduction in power consumption can be also observed in conventional vehicles driving in the same network. This phenomenon was demonstrated using two scenarios: platoon and urban network. In the first scenario, conventional vehicles imitate the driving style of eco-vehicles resulting in reduction of energy usage. More specifically, a strategy which incorporates both energy consumption and naturalistic driving style, leads to reduction in energy consumption above 10% in the first 11 vehicles of a platoon. Additionally, smaller values of acceleration and deceleration were observed in the ego-vehicles, implying more predictable velocity profiles which could contribute to improving road safety.

The analysis on the more realistic urban network was performed for different proportions of eco-vehicles and for two congestion levels. It was demonstrated that when traffic density in the network is high, even for small penetration rates of eco-vehicles, there is a reduction in energy consumption of other network participants. For low-density traffic conditions, the impact on conventional vehicles is negligible, but the effect is nonetheless positive if both types of vehicles are taken into account.

In a few cases, the eco-driving strategy did not result in an expected improvement. This is primarily due to the fact, that traffic lights changes are not taken into account in the optimisation aiming at power reduction. For this reason, future work will primarily focus on including such environmental factors into OCP. Furthermore, in the urban scenario, it was assumed that lead vehicles travel at constant speed for a short period of time. It is expected that the eco-driving strategy can be improved if the traffic prediction is incorporated in the optimisation. Inclusion of those extra factors will drastically increase the input dimension into GPR model, which will require additional algorithmic modifications incorporating low-dimensional reduction approaches.

References

[1] S. Wee, M. Coffman, and S. Allen, "Ev driver characteristics: Evidence from hawaii," *Transport Policy*, 2020.

[2] L. Hutchinson, B. Waterson, B. Anvari, and D. Naberezhnykh, "Potential of wireless power transfer for dynamic charging of electric vehicles," *IET intelligent transport systems*, vol. 13, no. 1, pp. 3–12, 2018.

[3] S. Kim, J. Lee, and C. Lee, "Does driving range of electric vehicles influence electric vehicle adoption?" *Sustainability*, vol. 9, no. 10, p. 1783, 2017.

[4] M. Coffman, P. Bernstein, and S. Wee, "Electric vehicles revisited: a review of factors that affect adoption," *Transport Reviews*, vol. 37, no. 1, pp. 79–93, 2017.

[5] K. Smith, M. Earleywine, E. Wood, and A. Pesaran, "Battery wear from disparate duty-cycles: Opportunities for electric-drive vehicle battery health management," National Renewable Energy Lab.(NREL), Golden, CO (United States), Tech. Rep., 2012.

[6] J. García-Villalobos, I. Zamora, J. I. San Martín, F. J. Asensio, and V. Aperribay, "Plug-in electric vehicles in electric distribution networks: A review of smart charging approaches," *Renewable and Sustainable Energy Reviews*, vol. 38, pp. 717–731, 2014.

[7] J. N. Barkenbus, "Eco-driving: An overlooked climate change initiative," *Energy Policy*, vol. 38, no. 2, pp. 762–769, 2010.

[8] M. A. S. Kamal, M. Mukai, J. Murata, and T. Kawabe, "On board eco-driving system for varying road-traffic environments using model predictive control," in *2010 IEEE International Conference on Control Applications*. IEEE, 2010, pp. 1636–1641.

[9] M. Knowles, H. Scott, and D. Baglee, "The effect of driving style on electric vehicle performance, economy and perception," *International Journal of Electric and Hybrid Vehicles*, vol. 4, no. 3, pp. 228–247, 2012.

[10] Y. Huang, E. C. Ng, J. L. Zhou, N. C. Surawski, E. F. Chan, and G. Hong, "Eco-driving technology for sustainable road transport: A review," *Renewable and Sustainable Energy Reviews*, vol. 93, pp. 596–609, 2018.

[11] M. Kuriyama, S. Yamamoto, and M. Miyatake, "Theoretical study on eco-driving technique for an electric vehicle with dynamic programming," in *2010 International Conference on Electrical Machines and Systems*. IEEE, 2010, pp. 2026–2030.

[12] R. Q. Malik, H. A. Alsattar, K. N. Ramli, B. Zaidan, A. Zaidan, Z. H. Kareem, H. A. Ameen, S. Garfan, A. Mohammed, and R. A. Zaidan, "Mapping and deep analysis of vehicle-to-infrastructure communication systems: coherent taxonomy, datasets, evaluation and performance measurements, motivations, open challenges, recommendations, and methodological aspects," *IEEE Access*, vol. 7, pp. 126 753–126 772, 2019.

[13] G. Mu, Z. Xinyu, L. Deyi, Z. Tianlei, and A. Lifeng, "Traffic light detection and recognition for autonomous vehicles," *The Journal of China Universities of Posts and Telecommunications*, vol. 22, no. 1, pp. 50–56, 2015.

[14] A. Sciarretta, G. De Nunzio, and L. L. Ojeda, "Optimal ecodriving control: Energy-efficient driving of road vehicles as an optimal control problem," *IEEE Control Systems Magazine*, vol. 35, no. 5, pp. 71–90, 2015.

[15] J. Hooker, "Optimal driving for single-vehicle fuel economy," *Transportation Research Part A: General*, vol. 22, no. 3, pp. 183–201, 1988.

[16] E. Ozatay, S. Onori, J. Wollaeger, U. Ozguner, G. Rizzoni, D. Filev, J. Michelini, and S. Di Cairano, "Cloud-based velocity profile optimization for everyday driving: A dynamic-programming-based solution," *IEEE Transactions on Intelligent Transportation Systems*, vol. 15, no. 6, pp. 2491–2505, 2014.

[17] L. Guo, B. Gao, Y. Gao, and H. Chen, "Optimal energy management for hevs in eco-driving applications using bi-level mpc," *IEEE Transactions on Intelligent Transportation Systems*, vol. 18, no. 8, pp. 2153–2162, 2016.

[18] M. Barth and K. Boriboonsomsin, "Energy and emissions impacts of a freeway-based dynamic eco-driving system," *Transportation Research Part D: Transport and Environment*, vol. 14, no. 6, pp. 400–410, 2009.

[19] W. Dib, A. Chasse, P. Moulin, A. Sciarretta, and G. Corde, "Optimal energy management for an electric vehicle in eco-driving applications," *Control Engineering Practice*, vol. 29, pp. 299–307, 2014.

[20] A. Vahidi and A. Sciarretta, "Energy saving potentials of connected and automated vehicles," *Transportation Research Part C: Emerging Technologies*, vol. 95, pp. 822–843, 2018.

[21] J. Fleming, X. Yan, C. Allison, N. Stanton, and R. Lot, "Driver modeling and implementation of a fuel-saving ADAS," in *IEEE Conference on Systems, Man and Cybernetics*, 2018.

[22] D. S. Puma-Benavides, J. Izquierdo-Reyes, J. d. D. Calderon-Najera, and R. A. Ramirez-Mendoza, "A systematic review of technologies, control methods, and optimization for extended-range electric vehicles," *Applied Sciences*, vol. 11, no. 15, p. 7095, 2021.

[23] Y. Zhang, J. Chen, T. You, Y. Zhang, Z. Liu, and C. Du, "Energy-aware optimization of connected and automated electric vehicles considering vehicle-traffic nexus," *IEEE Transactions on Industrial Electronics*, 2023.

[24] Y. Zhang, Y. Zhang, Z. Ai, Y. L. Murphey, and J. Zhang, "Energy optimal control of motor drive system for extending ranges of electric vehicles," *IEEE Transactions on Industrial Electronics*, vol. 68, no. 2, pp. 1728–1738, 2019.

[25] J. Peng, F. Zhang, S. Coskun, X. Hu, Y. Yang, R. Langari, and J. He, "Hierarchical optimization of speed planning and energy management for connected hybrid electric vehicles under multi-lane and signal lights aware scenarios," *IEEE Transactions on Intelligent Transportation Systems*, 2023.

[26] N. Zhao, F. Zhang, Y. Yang, S. Coskun, X. Lin, and X. Hu, "Dynamic traffic prediction-based energy management of connected plug-in hybrid electric vehicles with long short-term-state of charge planning," *IEEE Transactions on Vehicular Technology*, 2023.

[27] Y. Zhang, T. You, J. Chen, C. Du, Z. Ai, and X. Qu, "Safe and energy-saving vehicle-following driving decision-making framework of autonomous vehicles," *IEEE Transactions on Industrial Electronics*, vol. 69, no. 12, pp. 13 859–13 871, 2021.

[28] Y. Zhang, Z. Ai, J. Chen, T. You, C. Du, and L. Deng, "Energy-saving optimization and control of autonomous electric vehicles with considering multiconstraints," *IEEE Transactions on Cybernetics*, vol. 52, no. 10, pp. 10 869–10 881, 2021.

[29] Y. Zhang, Y. Zhang, Z. Liu, J. Chen, T. You, and C. Du, "An eco-cruise control for electric vehicles moving on slope road with constant speed," *Journal of Advanced Transportation*, vol. 2021, pp. 1–14, 2021.

[30] A. Garcia-Castro, A. Monzon, C. Valdes, and M. Romana, "Modeling different penetration rates of eco-driving in urban areas: Impacts on traffic flow and emissions," *International Journal of Sustainable Transportation*, vol. 11, no. 4, pp. 282–294, 2017.

[31] I. Kobayashi, Y. Tsubota, and H. Kawashima, "Eco-driving simulation: evaluation of eco-driving within a network using traffic simulation," *WIT Transactions on The Built Environment*, vol. 96, 2007.

[32] G. Qian and E. Chung, "Evaluating effects of eco-driving at traffic intersections based on traffic micro-simulation," *Evaluating effects of eco-driving at traffic intersections based on traffic micro-simulation*, pp. 1–11, 2011.

[33] H. Jiang, J. Hu, S. An, M. Wang, and B. B. Park, "Eco approaching at an isolated signalized intersection under partially connected and automated vehicles environment," *Transportation Research Part C: Emerging Technologies*, vol. 79, pp. 290–307, 2017.

[34] Y. He, M. Chowdhury, Y. Ma, and P. Pisu, "Merging mobility and energy vision with hybrid electric vehicles and vehicle infrastructure integration," *Energy Policy*, vol. 41, pp. 599–609, 2012.

[35] X. He and X. Wu, "Eco-driving advisory strategies for a platoon of mixed gasoline and electric vehicles in a connected vehicle system," *Transportation Research Part D: Transport and Environment*, vol. 63, pp. 907–922, 2018.

[36] J. Liu, K. Kockelman, and A. Nichols, "Anticipating the emissions impacts of smoother driving by connected and autonomous vehicles, using the moves model," in *Transportation Research Board 96th Annual Meeting*, 2017.

[37] X. Yan, J. Fleming, and R. Lot, "Fuel economy and naturalistic driving for passenger road vehicles," in *2018 IEEE Vehicle Power and Propulsion Conference (VPPC)*. IEEE, 2018, pp. 1–6.

[38] M. Treiber, A. Hennecke, and D. Helbing, "Congested traffic states in empirical observations and microscopic simulations," *Physical review E*, vol. 62, no. 2, p. 1805, 2000.

[39] J. Fleming, X. Yan, and R. Lot, "Incorporating driver preferences into eco-driving assistance systems using optimal control," *IEEE Transactions on Intelligent Transportation Systems*, 2020.

[40] C. K. Williams and C. E. Rasmussen, *Gaussian processes for machine learning*. MIT press Cambridge, MA, 2006, vol. 2 (3).

[41] W. Zhao, D. Ngoduy, S. Shepherd, R. Liu, and M. Papageorgiou, "A platoon based cooperative eco-driving model for mixed automated and human-driven vehicles at a signalised intersection," *Transportation Research Part C: Emerging Technologies*, vol. 95, pp. 802–821, 2018.

[42] C. Chen, J. Wang, Q. Xu, J. Wang, and K. Li, "Mixed platoon control of automated and human-driven vehicles at a signalized intersection: dynamical analysis and optimal control," *Transportation research part C: emerging technologies*, vol. 127, p. 103138, 2021.

[43] U. G. D. Transport, "Veh0104: Licensed vehicles by body type, by region and per head of population: Great britain and united kingdom," 2017.

[44] J. Kim and H. S. Mahmassani, "Correlated parameters in driving behavior models: Car-following example and implications for traffic microsimulation," *Transportation research record*, vol. 2249, no. 1, pp. 62–77, 2011.

[45] J. Monteil, R. Billot, J. Sau, C. Buisson, and N.-E. E. Faouzi, "Calibration, estimation, and sampling issues of car-following parameters," *Transportation research record*, vol. 2422, no. 1, pp. 131–140, 2014.

[46] V. Punzo, B. Ciuffo, and M. Montanino, "Can results of car-following model calibration based on trajectory data be trusted?" *Transportation research record*, vol. 2315, no. 1, pp. 11–24, 2012.
[47] X. Yan, J. Fleming, C. Allison, and R. Lot, "Portable automobile data acquisition module (adam) for naturalistic driving study," 2017.
[48] D. A. Hensher and K. J. Button, *Handbook of transport modelling*. Emerald Group Publishing Limited, 2007.
[49] P. Robillard, "Estimating the od matrix from observed link volumes," *Transportation Research*, vol. 9, no. 2-3, pp. 123–128, 1975.
[50] C. Katrakazas, M. Quddus, and W.-H. Chen, "A new integrated collision risk assessment methodology for autonomous vehicles," *Accident Analysis & Prevention*, vol. 127, pp. 61–79, 2019.
[51] E. W. Dijkstra, "A note on two problems in connection with graphs," *Numerische mathematik*, vol. 1, no. 1, pp. 269–271, 1959.
[52] C. B. Rafter, B. Anvari, S. Box, and T. Cherrett, "Augmenting traffic signal control systems for urban road networks with connected vehicles," *IEEE Transactions on Intelligent Transportation Systems*, vol. 21, no. 4, pp. 1728–1740, 2020.
[53] S. Saini, S. Nikhil, K. R. Konda, H. S. Bharadwaj, and N. Ganeshan, "An efficient vision-based traffic light detection and state recognition for autonomous vehicles," in *2017 IEEE Intelligent Vehicles Symposium (IV)*. IEEE, 2017, pp. 606–611.
[54] https://github.com/cbrafter/SUMO_FRAMEWORK.
[55] https://github.com/jakubkrol/network_effects.

Jakub Krol has received his BSc & MSc degrees in Aeronautical Eng. in 2013 at Imperial College London. Subsequently, he has obtained his PhD degree in 2017 in the same department, with the research topics focusing on applications of different dimensional reduction techniques to dynamic estimation & reconstruction of bluff body flows. After a brief stint as a quantitative analyst in a proprietary trading firm, Jakub has decided to go back to academia and currently works as a Research Fellow in the Intelligent Mobility Group/Lab at UCL (IM@UCL). His primary research interests include data-driven dynamical modelling, estimator design & applications of machine learning to engineering problems.

Bani Anvari is a Professor of Intelligent Mobility at UCL. She is the research leader of the Intelligent Mobility Group and Director of IM Lab at UCL (IM @UCL). She is interested in the complexity of interactions and how intuitive, intelligent, human-centric and personalised control systems can influence it. Her research focus has been on Intelligent Mobility, with an emphasis on exploring driver and pedestrian interaction with semi- and fully-autonomous vehicles in different contexts (e.g., shared spaces, CAVs), an area of application that significantly benefits from Robotics and AI.

Craig Rafter received the M.E. in Electronics and Computer Engineering from University College Dublin in 2015. He has completed the Engineering and Physical Sciences Research Council centre for doctoral training in Next Generation Computational Modelling. He was awarded a PhD for investigating the effects of traffic signal control using connected vehicle data on the transport network by the University of Southampton Transportation Research Laboratory. He is now a Senior Applied Scientist at Improbable. asdsad

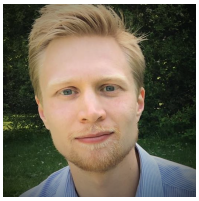

James Fleming is a Lecturer within the Wolfson School of Mechanical, Electrical and Manufacturing Engineering at Loughborough University, joining the school in September 2019. James obtained the MEng and DPhil degrees in 2012 and 2016 respectively from the University of Oxford, where he studied control engineering and developed algorithms for Model Predictive Control of uncertain state-space systems as part of his doctoral research. From 2016 to 2019 he was a Research Fellow at the University of Southampton, developing driver models and optimal control algorithms for the G-Active (Green, Adaptive ConTrol of Interconnected VEhicles) project, which used knowledge of driver preferences to save fuel and reduce emissions in the energy management of conventional, hybrid and electric vehicles.

Xingda Yan is a Senior New Product Definition Engineer at Power Electronics & Control Specialist. He is an experienced researcher with a demonstrated history of working in the automotive sector. Skilled in control system design for electrical and electronics application, Mathematical modelling and optimisation, C++, FPGA prototyping, and LaTeX. Strong research professional with a Doctor of Philosophy (Ph.D.) focused on power electronics from University of Southampton.

Roberto Lot is Professor of Mechanics of Machines at Universit degli Studi di Padova. He has significant experience in the motorcycles dynamics and control field, his research interest includes handling, comfort, safety systems, vehicle performance, driving simulators applied to a range of vehicles from small scooter to racing motorcycles, comprising also electric and three-wheeled vehicles. He has led research projects founded by public organization and industries at national and international level, and published about 100 scientific articles.